land

MDPI

Article

Remote Sensing Monitoring and Spatial Pattern Analysis of Non-Grain Production of Cultivated Land in Anhui Province, China

Junjun Zhi [1,2], Xinyue Cao [1], Wangbing Liu [3,*], Yang Sun [1], Da Xu [4], Caiwei Da [1], Lei Jin [3], Jin Wang [3], Zihao Zheng [5], Shuyuan Lai [1], YongJiao Liu [1] and Guohai Zhu [1]

1 School of Geography and Tourism, Anhui Normal University, Wuhu 241002, China; zhijunjun@ahnu.edu.cn (J.Z.); caoxy2021@ahnu.edu.cn (X.C.); syyjl2140@ahnu.edu.cn (Y.S.); dcw0821@ahnu.edu.cn (C.D.); lsy007@ahnu.edu.cn (S.L.); lyj1106@ahnu.edu.cn (Y.L.); zgh111@ahnu.edu.cn (G.Z.)
2 Engineering Technology Research Center of Resources Environment and GIS, Anhui Province, Wuhu 241002, China
3 Key Laboratory of Jianghuai Arable Land Resources Protection and Eco-Restoration, Hefei 230088, China; m15256592757@163.com (L.J.); 18919606707@163.com (J.W.)
4 Urban and Rural Planning Management Service Center of Jin'an District, Lu'an 237100, China; chenjialu@whu.edu.cn
5 College of Letters and Science, University of California, Santa Barbara, CA 93106, USA; zihaozheng@ucsb.edu
* Correspondence: qinting@ahnu.edu.cn

Abstract: In recent years, non-grain production of cultivated land (NGPCL) has become increasingly prominent in China, seriously affecting food production and threatening the country's food security. However, there is a lack of large-scale and high-precision methods for remote sensing identification of NGPCL. From the perspective of effective management of cultivated land resources, the characteristics of the spatial patterns of NGPCL, both on a large scale and at a patch scale, need to be further studied. For solving this problem, this paper uses the Google Earth engine (GEE) cloud computing platform and multi-source remote sensing data with a machine learning algorithm to determine the occurrence of NGPCL in Anhui province in 2019, and then uses nine selected landscape pattern indexes to analyze the spatial patterns of NGPCL from two aspects, specifically, economic development level and topography. The results show that: (1) terrain features, radar features, and texture features are beneficial to the extraction of NGPCL; (2) the degree of separation obtained by using an importance evaluation approach shows that spectral features have the highest importance, followed by index features with red edges, texture features, index features without red edges, radar features, and terrain features; and (3) the cultivated land in Anhui province in 2019 is mainly planted with food crops, and the phenomenon of NGPCL is more likely to occur in areas with high economic development levels and flat terrain. Aided by the GEE cloud platform, multi-source remote sensing data, and machine learning algorithm, the remote sensing monitoring approach utilized in this study could accurately, quickly, and efficiently determine NGPCL on a regional scale.

Keywords: non-grain production; Google Earth engine; remote sensing; landscape pattern; land use; cultivated land

Citation: Zhi, J.; Cao, X.; Liu, W.; Sun, Y.; Xu, D.; Da, C.; Jin, L.; Wang, J.; Zheng, Z.; Lai, S.; et al. Remote Sensing Monitoring and Spatial Pattern Analysis of Non-Grain Production of Cultivated Land in Anhui Province, China. *Land* **2023**, *12*, 1497. https://doi.org/10.3390/land12081497

Academic Editor: Rui Alexandre Castanho

Received: 29 June 2023
Revised: 23 July 2023
Accepted: 25 July 2023
Published: 28 July 2023

1. Introduction

Cultivated land is of great importance for grain production [1–3]. At present, the global population has exceeded 7.8 billion and it is expected to continue to grow in the next several decades, which leads to higher requirements for food production and supply [4]. China has a large population, 1.4 billion, and food self-sufficiency is very important. As early as 2006, in order to ensure national food security, "1.8 billion mu (0.12 billion ha) of cultivated land" had become an obligatory indicator and an insurmountable red line. However, in recent years, the phenomenon of non-grain production of cultivated land (NGPCL, which refers to the agricultural production behavior of land managers using cultivated land for non-grain production purposes) has become increasingly prominent in China and has attracted great attention both from governments and researchers [1,5]. Such a problem, if not regulated by the government, will seriously endanger national food security [6].

In recent years, as governments around the world have paid increasing attention to the problem of NGPCL, this matter has gradually attracted the attention of researchers [7,8]. In this context, some developed countries have adopted digital tools to monitor the growth of crops on cultivated land. For instance, the U.S. Department of Agriculture has established a cropland data layer to monitor agricultural land annually [9,10]. Canada has published a digital map of crop types covering the country with a spatial resolution of 30 m since 2011 [11]. In China, current research on the identification of NGPCL mainly focuses on the macro analysis method using statistical data and the land parcel identification method based on remote sensing images and land survey data [12–14]. In terms of influencing factors, scholars pay more attention to cultivated land transfer behavior factors and economic factors [15–19]. In addition, some scholars focus on the management policies of NGPCL [20–23]. However, researchers have paid less attention to the dynamic remote sensing monitoring of NGPCL, which is of great importance for effective management of cultivated land resources [8,24,25].

The traditional method for determining the area of NGPCL mainly relies on manual surveys and statistical means through actual ground surveys, which are usually costly and time-consuming [8]. Such a traditional method cannot meet the actual needs of fine management for cultivated land [26,27]. Fortunately, the rapid development of remote sensing technology and Google Earth engine (GEE) cloud computing platform provide the possibility of accurately and rapidly extracting NGPCL information [24,25,28]. Additionally, there are few studies on the analysis of the characteristics of NGPCL from a spatial perspective. Since the phenomenon of NGPCL is related to many factors, such as natural conditions and regional economic and social development, it is difficult to explain the relationships between the characteristics of NGPCL and its influencing factors, and it is also difficult to formulate differential management policies, without accurate spatial difference information to inform the macro analysis of the characteristics of NGPCL. Therefore, it is particularly important to grasp the spatial characteristics of NGPCL on a regional scale.

This study aims to rapidly identify NGPCL on the patch scale and accurately analyze its spatial characteristics on a regional scale. The specific research objectives are as follows: (1) to achieve rapid and high-precision identification of the spatial distribution of NGPCL in Anhui province, China, in 2019 by using a variety of remote sensing data and the machine learning method on the GEE remote sensing cloud computing platform; and (2) to reveal the differentiated spatial characteristics of NGPCL in Anhui province in 2019 under different economic development levels and topographical conditions using various spatial analysis approaches, including zonal statistics and landscape pattern analysis. This study will provide a scientific reference for rapidly determining NGPCL on the regional scale by using remote sensing cloud platform based monitoring technology. Moreover, the revelation of the spatial distribution characteristics of NGPCL will help governments to formulate targeted policies.

2. Materials and Methods

2.1. Study Area

Anhui province (29°41′–34°38′ N and 114°54′–119°37′ E) is located in the Yangtze River Delta in East China with a total area of 140,100 km^2 (Figure 1). There are four types of terrain in Anhui province, specifically, plain, platform, hill, and mountain. The whole province can be divided into five geomorphological regions, i.e., the Huaihe Plain, the Jianghuai Platform, the West Anhui Hills, the Riverside Plains, and the South Anhui Hills and Mountains, occupied by 30.48%, 17.56%, 9.99%, 24.91%, and 16.70% of the total area, respectively. In 2019, the sown area of grain in Anhui province was slightly reduced while the sown area of economic crops increased compared with those in 2018. The annual grain output was 40.54 million tons with an increase of 1.2%, ranking fourth in the country, making an important contribution to domestic food security.

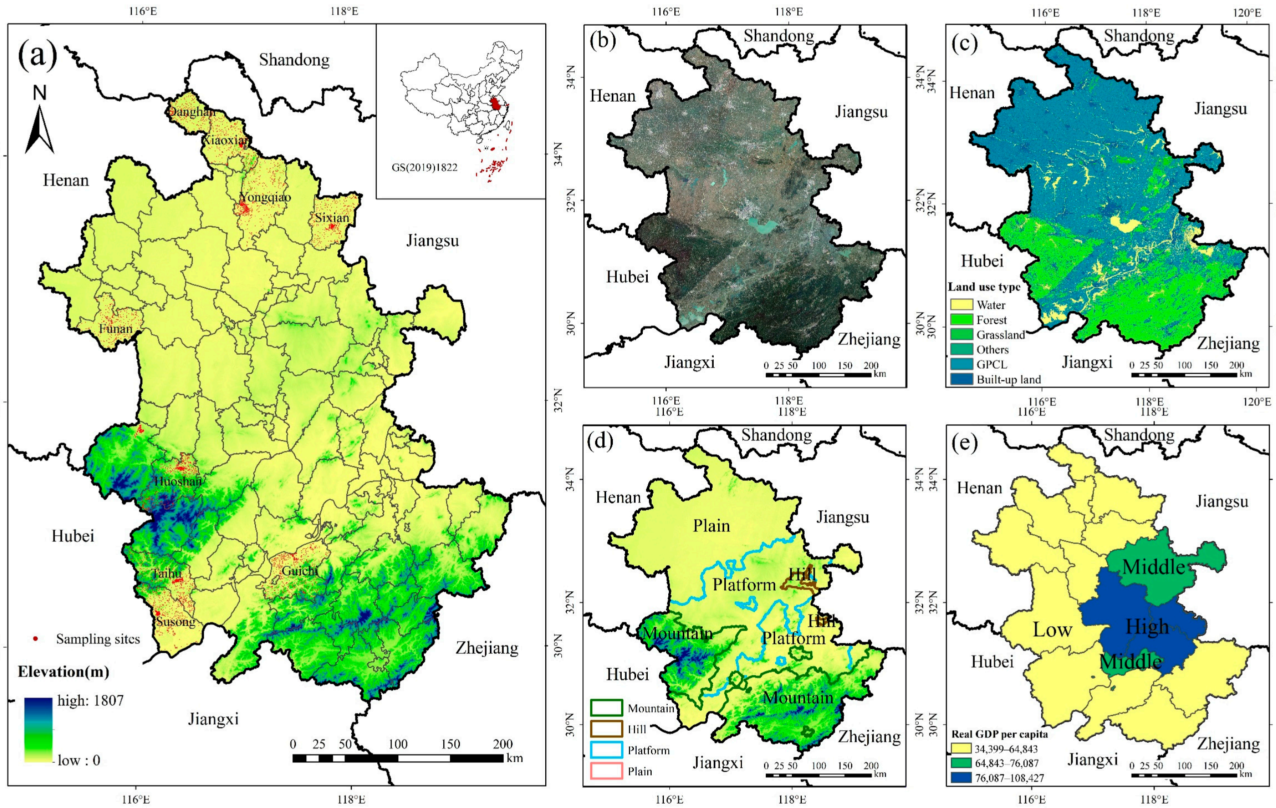

Figure 1. Study area (Anhui province, China). (**a**) Study area with elevation information and locations of sampling sites; (**b**) remote sensing image (comprising the RGB bands of Sentinel-2 images); (**c**) land use/land cover in 2019; (**d**) terrain types of the study area; and (**e**) spatial difference in the economic development of the study area in 2019.

In recent years, driven by the non-standard management of agricultural land with facilities, the low income of grain planting, the accelerated process of land transfer, and the considerable income of planting cash crops, the phenomenon of NGPCL in Anhui province is widespread. However, there is a lack of mature technology for rapid and effective intervention and management. Currently, the agricultural development goal of Anhui province is accelerating the transformation from a "big agricultural province" to a "powerful agricultural province", thus, choosing Anhui province as the research area is typical and representative, and has strong practical significance.

2.2. Data Sources

Five types of data are used in this study, including optical remote sensing images, terrain, statistical data, field survey data, and administrative boundary (Table 1). Optical remote sensing images, terrain, and radar data are taken directly from the GEE platform, including Sentinel-1 images, Sentinel-2 MSI images, and Google Earth high-resolution images. Sentinel-1 and Sentinel-2 MSI images are used to identify land use types in the study area in 2019. Due to the huge data volume of the study area (140,100 km^2) and the influence of cloud pollution, it is difficult to obtain single-phase satellite images covering the whole extent of the study area. Therefore, the optical synthetic image was created using the satellite images obtained during the period from May to August in 2019, which provides the most cloud-free data and is in accordance with the optimal period of food crop rotation for retaining sufficient crop information. For synthesizing cloud-free images, the percentage of cloud cover is set below 20%, and the Sentinel-2 cloud mask algorithm and the median synthesis method are used to reconstruct minimal cloud cover composite image (Figure 2). To benefit data calculation and the management mechanism of the GEE platform [29], all remote sensing data used in this study were sampled at 10-m resolution. Moreover, GEE unifies the co-ordinate system through the embedded algorithm to ensure geometric registration accuracy between different data sources [30]. Google Earth high-resolution images were used for visual inspection of land use classification results in 2019 and sampling sites; SRTM V3 data were used as terrain data, which was mainly used to obtain four terrain indexes: elevation, slope, aspect, and mountain shadow. The statistical data included the per capita GDP data of each city and were obtained from the *2019 Anhui Provincial Statistical Yearbook*. The landform zoning data used for dividing the topography in Anhui were taken from the spatial distribution data of 1:1 million landform types in China.

The sampling site data came from national land survey data, geographic national conditions monitoring data, and actual field survey data, including Huoshan county, Si county, Xiao county, Dangshan county, Yongqiao district, Funan county, Guichi district, Susong county, and Taihu county (Figure 3). The total number of sampling sites was 6500, including 800 sampling sites for each land use type of grassland, water, abandoned cultivated land, garden land, forest, and built-up land, and 850 sampling sites for each of the GPCL and NGPCL. The ratio of sampling sites for training and validation was 7:3 [31], which were 4550 and 1950 sampling sites, respectively.

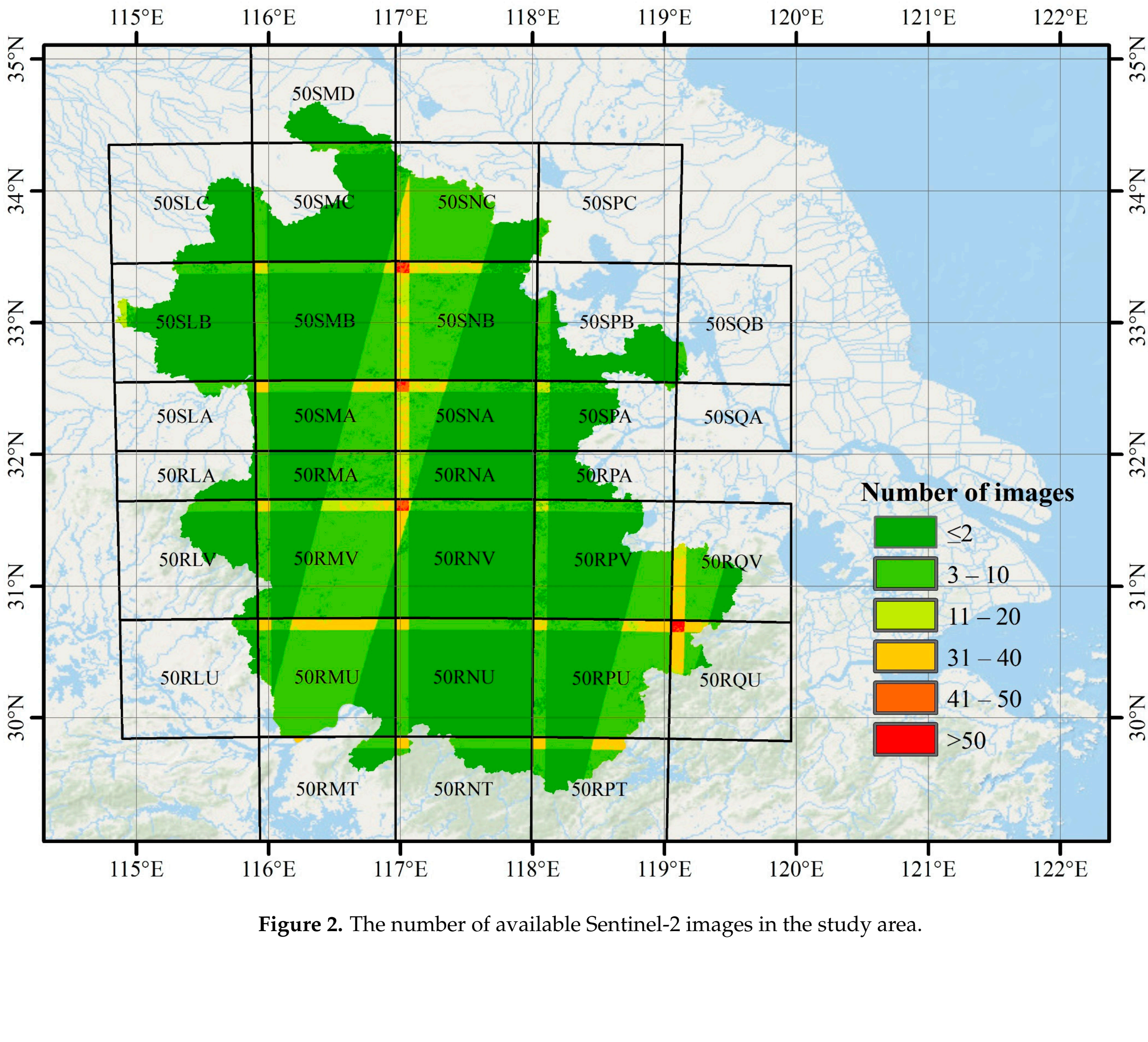

Figure 2. The number of available Sentinel-2 images in the study area.

Table 1. Type of data.

Data Type	Data Name	Scale	Application	Source
Radar data Optical remote sensing image data	Sentinel-1 Radar Data (GRD products)	10 m	Improve the classification accuracy of crops	https://developers.google.com/earth-engine/datasets/catalog/COPERNICUS_S1_GRD (accessed on 7 May 2022).
	Sentinel-2 MSI	10 m	Identify NGPCL and other land use types	https://developers.google.com/earth-engine/datasets/catalog/sentinel-2 (accessed on 5 July 2021).
Terrain data	SRTM V3	30 m	Extract terrain features	NASA SRTM1 v3.0
Statistical data	2019 per capita GDP data of each city in Anhui province	/	Economic zoning	http://tjj.ah.gov.cn/oldfiles/tjj/tjjweb/tjnj/2019/cn.html (accessed on 1 June 2022).
Vector data	Administrative boundary	/	Zonal statistics	https://www.webmap.cn/main.do?method=index (accessed on 10 July 2021).
Field survey data	Sample point	/	Create training samples and validation samples	/

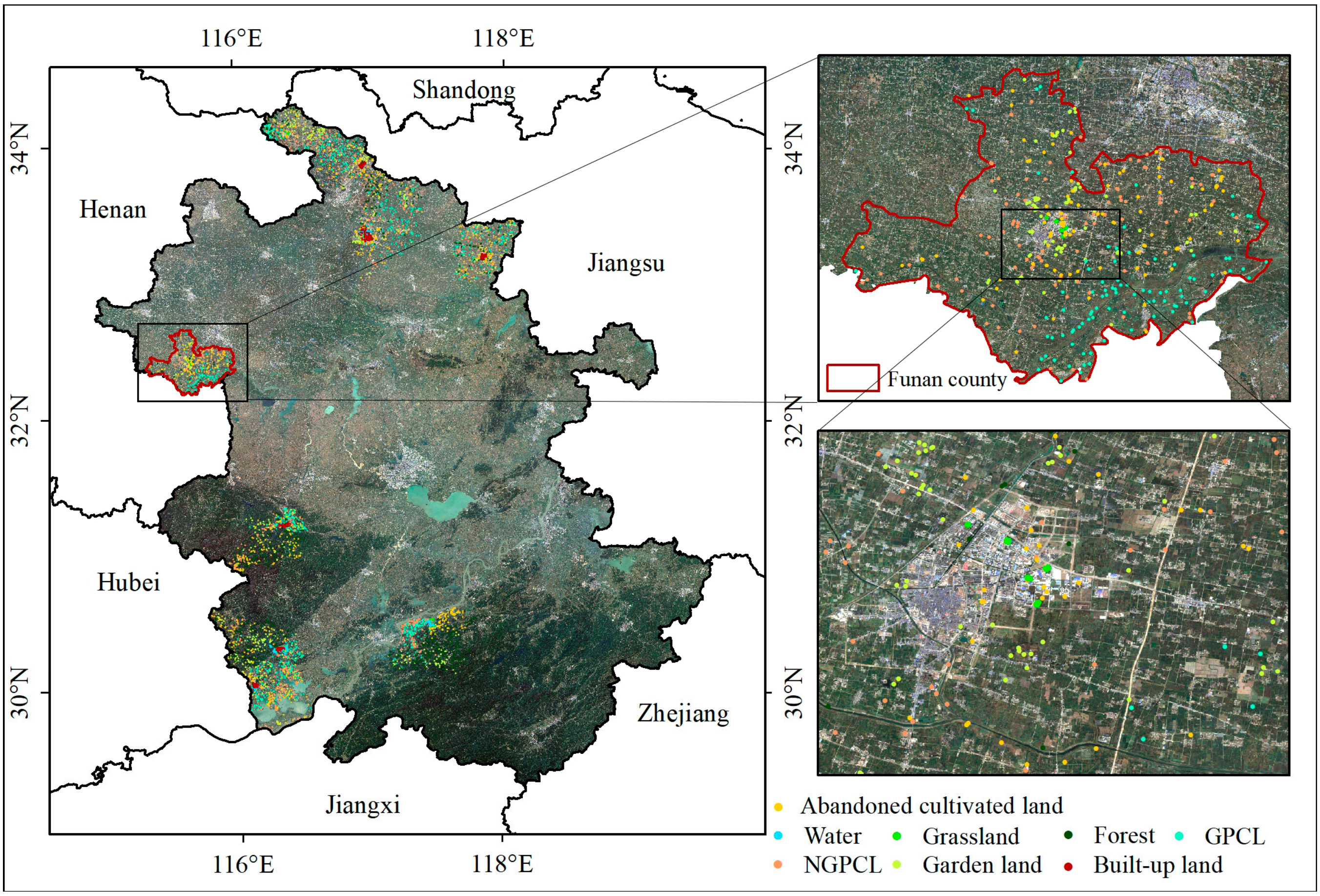

Figure 3. Distribution map of sample points in the study area.

2.3. Methods

2.3.1. Research Framework

Figure 4 shows the technical flowchart illustrating the methodology adopted in the present study. The random forest algorithm was utilized to extract NGPCL in Anhui province in 2019 and to analyze its spatial patterns. Based on freely available Sentinel-1 radar data and Sentinel-2 optical remote sensing images obtained from the GEE platform, spectral features, texture features, terrain features, and other features were first generated, and the random forest algorithm was used to optimize these features for obtaining the optimal combination of features for classification, and, also, the random forest algorithm was used to parameterize the classification model. Six different classification feature composition schemes were built and then performed by the random forest-based classification model. The accuracies of six different classification feature composition schemes were compared, and the optimal classification result adopted to analyze the spatial patterns of NGPCL in Anhui province in 2019 with the landscape index.

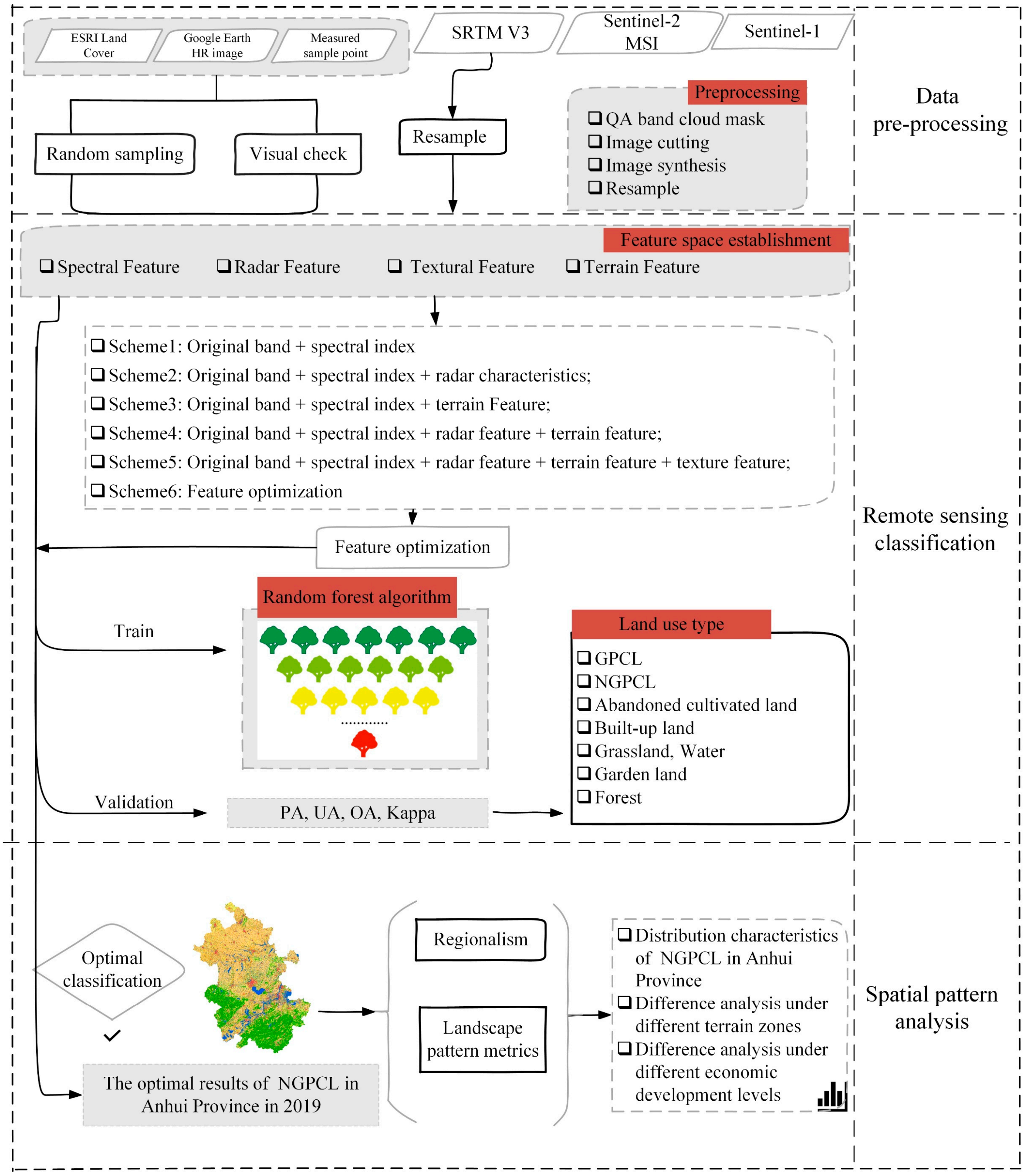

Figure 4. Flowchart illustrating the methodology adopted in the present study.

2.3.2. Feature Set Construction

This study considered the use of spectral features, texture features, terrain features, and radar features for feature set construction (Table 2).

Table 2. Feature Description.

Variable	Abbreviation	Feature Description	Citation
Spectral features	B	B1–B4, B8, B8a, B9–B12	[13]
Spectral index feature without red-edged band	NDVI	(B8-B4)/(B8 + B4)	[13]
	NDWI	(B3-B8)/(B3 + B8)	[32]
	MNDWI	(B3-B11)/(B11 + B3)	[33]
	NDBI	(B11-B8)/(B11 + B8)	[34]
	MNDBI	(B12-B8)/(B12 + B8)	[35]
	RVI	B8/B4	[36]
	DVI	B8-B4	[37]
	EVI	2.5 × (B8-B4)/(B8 + 6 × B4-7.5 × B2 + 1)	[32]
	LSWI	(B8-B11)/(B8 + B11)	[36]
	BSI	[(B12 + B4)-(B8-B2)]/[(B12 + B4) + (B8-B2)]	[13]
	SAVI	(B8-B4) × (1 + 0.5)/(B8 + B4 + 0.5)	[13]
Spectral index features with red-edged band	RNDVI	(B8-B5)/(B8 + B5)	[38]
	RRVI	B8/B5	[39]
	RDVI	B8-B5	[40]
	MCARI	((B5-B4)-0.2× (B5-B3)) × (B5-B4)	
	NDVIre1	(B8A-B5)/(B8A + B5)	[41]
	NDVIre2	(B8A-B6)/(B8A + B6)	
	NDVIre3	(B8A-B7)/(B8A + B7)	
	NDre1	(B6-B5)/(B6 + B5)	
	NDre2	(B7-B5)/(B7 + B5)	
	CIre	B7/B5-1	
	NBR	(B8-B12)/(B8 + B12)	[13]
Terrain features	Elevation	/	[42]
	Slope	/	
	Aspect	/	
	Hillshade	/	
Radar signature	VV	/	[43]
	VH	/	
Texture features	"CORR", "ASM", "ENT", "IDM", "SHADE", "SAVG", "IMCORR1", "SENT", "DENT", "VAR1", "SVAR", "DVAR", "MAXCORR", "DISS", "INERTIA", "PROM", "IMCORR2"	/	[44,45]

2.3.3. Feature Optimization

This study compared six different classification feature composition schemes from different dimensions of features to explore their influence on the classification results. The six different classification schemes were: (1) original band + spectral index; (2) original band + spectral index + radar feature; (3) original band + spectral index + terrain feature; (4) original band + spectral index + radar feature + terrain feature; (5) original band + spectral index + radar feature + terrain feature + texture feature; and (6) optimal features obtained by feature optimization.

The explain function in GEE was used to calculate the relative importance of each factor by using the RF algorithm, and the least important factor was removed one by one, and then we built a new random forest model and recalculated the model performance and the relative importance of each factor retained in each step. The out-of-bag (OOB) error index was used to assess the classification accuracy of each model, and the factors used in the random forest model were taken as the optimal factors when the OOB error reachesd the minimum.

2.3.4. Random Forest Algorithm

The random forest classifier has the advantages of high robustness, fast classification speed, and good data compatibility, and is widely used in land use classification, data mining, and other fields [46]. The result of random forest classifier comes from the result of multiple decision trees aggregated by majority voting. The random forest classifier has strong predictive performance. It has strong robustness and is usually not prone to overfitting. Moreover, it has the advantages of low deviation and low variance, and is suitable for processing high-dimensional data sets, especially when using a large number of samples [47,48]. Thus, the random forest classifier was used for the determination of NGPCL.

The size of the training sample set has been found to directly affect the performance of the random forest classifiers [49]. Therefore, a large number of sampling sites (6500) were used for classification to obtain stable results. The ee.Classifier.smileRandomForest function was used in GEE to execute the classification. Such a function needs to set two parameters, including the number of decision trees (number of trees) and the number of child nodes (min leaf population). The number of decision trees was set to 500 with 50 set as the step size. The obtained classification accuracy was stable, with a variation of ±0.002.

2.3.5. Landscape Pattern Analysis

The landscape pattern index of cultivated land is an expression of the spatial pattern information of cultivated land, which effectively reflects the structural composition and spatial distribution characteristics of cultivated land resources (Table 3). For effective landscape pattern analysis, the classification result map was resampled to 200 m × 200 m, and, then, the landscape pattern analysis software Fragstats 4.2 was utilized to calculate the landscape pattern characteristics of land use types at the patch level.

Table 3. Descriptions of landscape pattern indexes.

Index	Calculation Formula	Meaning	Citation
CA	/	The area of a single class	/
$PLAND$	$PLAND = \frac{\sum_{j=1}^{n} a_{ij}}{A} \times 100\%$	The relative proportion of a certain patch type in the landscape to the entire landscape area, which is used to measure the type composition and relative size of the landscape	[50]
LPI	$LPI = \frac{a_{max}}{A} \times 100\%$	Used to determine the dominant patch types in the landscape, which indirectly reflects the direction and size of human disturbance	[51]
NP	/	Number of patches	/
PD	$PD = NP/A$	Expressing the density of a certain patch in the landscape, reflecting the overall heterogeneity and fragmentation of the landscape	[51]
$AREA\_{MN}$	$AREA\_{MN} = CA/n$	Average area of patches or types in the landscape	[51]
$COHESION$	$COHESION = \left(1 - \frac{\sum_{j=1}^{m} P_{ij}}{\sum_{j=1}^{m} P_{ij}\sqrt{a_{ij}}}\right) \frac{1}{1 - \frac{1}{\sqrt{A}}} \times 100\%$	Measure the degree of natural connectivity of the corresponding type, reflecting patch connectivity	[51]
$PROX\_{MN}$	$PROX\_{MN} = \sum_{i=1}^{n} \left(\frac{S_i}{Z_i}\right)$	Describe the spatial relationship between a habitat patch and its neighbors	[52]
FRAC_AM	/	Reflect the overall characteristics of the landscape pattern, also reflect the impacts of human activities	[53]

2.3.6. Accuracy Assessment

In this study, the accuracy of classification results was measured by the overall accuracy (OA), the kappa coefficient, the producer's accuracy, and the user's accuracy [54]. The overall accuracy is the ratio of the sum of correctly classified pixels to the total number of pixels, as shown in Formula (1). The kappa coefficient represents the ratio of error reduction between classification and completely random classification, as shown in Formula (2). The PA (producer's accuracy) refers to the ratio between the number of pixels correctly classified in a class and the number of all verified samples in that class. The UA (user's accuracy) refers to the ratio of the number of pixels correctly classified in a class to all pixels assigned to that class.

$$\mathrm{OA} = \frac{\sum_i^r x_{ii}}{\mathrm{n}} \tag{1}$$

$$\mathrm{Kappa} = \frac{\frac{\sum_i^{\mathrm{r}} x_{ii}}{\mathrm{n}} - \frac{\sum_{i=1}^{\mathrm{r}} \mathrm{x}_{i+} * \mathrm{x}_{+i}}{\mathrm{n}^2}}{1 - \frac{\sum_{i=1}^{\mathrm{r}} \mathrm{x}_{i+} * \mathrm{x}_{+i}}{\mathrm{n}^2}} \tag{2}$$

where, n is the total number of samples, r is the number of types, x_{ii} is the number of type combinations on the diagonal, x_{i+} is the total number of observations in rows, and x_{+i} is the total number of observations in columns.

3. Results

3.1. Classification Results Using Different Feature Combination Schemes

The classification results using six different feature combination schemes are shown in Tables 4 and 5 and Figures 5 and 6. The classification models using the three schemes of original band + spectral index + radar feature + terrain feature (Scheme4), original band + spectral index + radar feature + terrain feature + texture feature (Scheme5), and feature optimization (Scheme6) have higher average verification accuracies, while the accuracies of the classification model using the three feature combination schemes of original band + spectral index (Scheme1), original band + spectral index + radar feature (Scheme2), and original band + spectral index + terrain feature (Scheme3) are relatively low. The results show that terrain features, radar features, and texture features are conducive to the extraction of NGPCL. Compared with the classification accuracy of Scheme1 using original band + spectral features, the OA of Scheme5 with adding terrain features, radar features, and texture features increases by 1.5%, while PA and UA of NGPCL improved by 0.1% and 2.3%, PA and UA of abandoned cultivated land improved by 3% and 2.7%, and PA and UA for land with NGPCL by 2.3%, respectively.

Table 4. Classification results using different feature combination schemes.

Type		Grassland	Water	Abandoned Cultivated Land	Garden Land	Forest	GPCL	NGPCL	Built-Up Land	OA (%)	Kappa
Scheme1	PA/%	87.9	96.6	62.9	76.0	82.6	85.8	69.5	95.4	82.1	0.80
	UA/%	75.2	96.9	75	74.7	85.8	85.0	71.4	92.2		
Scheme2	PA/%	89.4	96.4	62.7	76.7	82.5	86.0	68.9	95.8	82.3	0.80
	UA/%	74.9	96.9	76.5	73.8	86.0	86.4	70.9	93.1		
Scheme3	PA/%	89.4	96.8	64.8	75.8	84.5	86.0	71.6	95.8	83.1	0.81
	UA/%	80.1	97.6	78.3	73.0	88.7	84.5	70.5	92.2		
Scheme4	PA/%	89.6	96.6	66.3	77.7	85.1	86.7	71.4	95.4	83.6	0.81
	UA/%	80.4	97.1	77.5	74.5	89.0	86.1	70.8	93.7		
Scheme5	PA/%	90.8	96.0	65.9	77.7	84.5	87.7	69.6	96.3	83.6	0.81
	UA/%	79.2	96.9	77.7	72.7	87.5	87.6	73.7	92.8		
Scheme6	PA/%	90.8	96.8	66.5	77.9	85.1	88.1	71.9	96.2	84.2	0.82
	UA/%	80.2	97.1	78.7	76.0	87.9	87.6	72.7	92.4		

Table 5. Confusion matrix of the classification results using the optimal feature combination scheme (Scheme6).

	Grassland	Water	Abandoned Cultivated Land	Garden Land	Forest	GPCL	NGPCL	Built-Up Land
Grassland	481	1	6	8	0	1	20	13
Water	0	538	3	3	0	1	3	8
Abandoned cultivated land	45	3	355	34	19	10	53	15
Garden land	11	0	27	408	31	15	31	1
Forest	10	1	9	35	451	8	15	1
GPCL	4	5	10	15	5	496	28	0
NGPCL	37	6	37	34	6	35	410	5
Built-up land	12	0	4	0	1	0	4	525

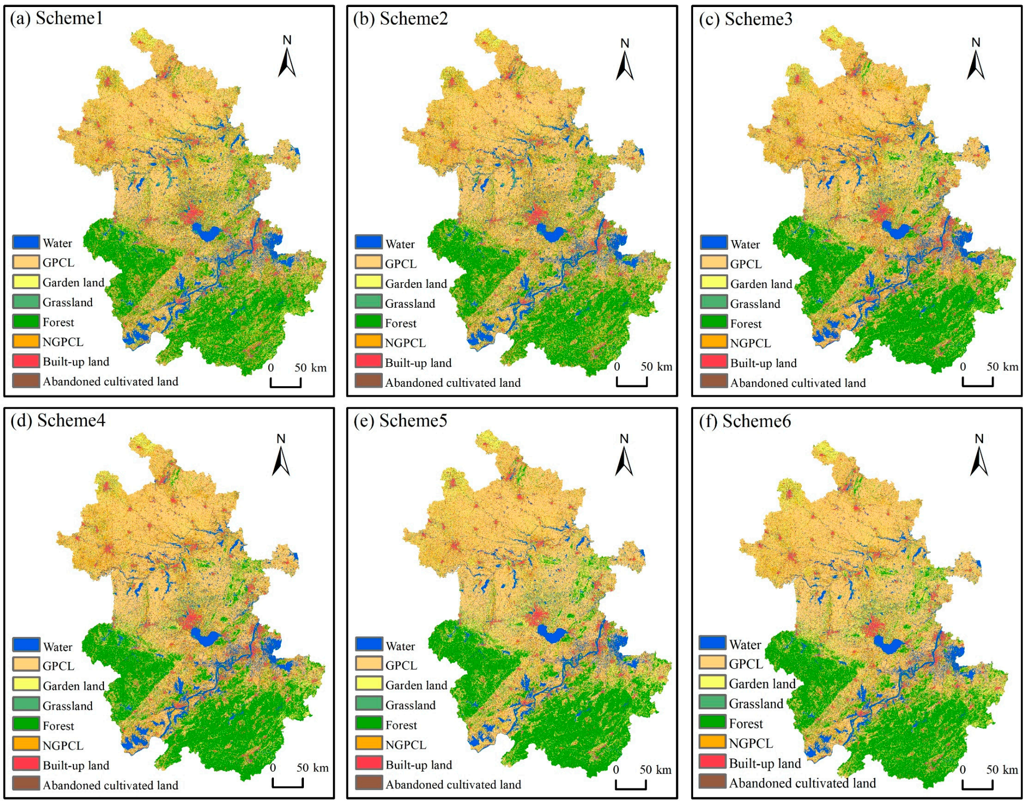

Figure 5. Classification results using different feature combination schemes.

3.2. Feature Importance Determined by Using Feature Optimization Approach

In this study, a total of 57 features (i.e., 12 original spectral bands, 11 non-red-edge spectral indices, 11 red-edge spectral indices, 4 terrain features, 2 radar features, and 17 texture features) were utilized for comparisons among the six different feature combination schemes. The optimal feature combination scheme (Scheme6) was determined by the comparison with classification accuracy. The importance of 34 features used for Scheme6 was determined by the random forest algorithm, which is shown in Figure 7. Compared with Scheme5 using all of the 57 features, the number of features used for Scheme6 significantly decreased by 41.4% while the OA and the Kappa improved by 0.6% and 0.1%, respectively. Especially, PA improved by 0.4% for GPCL, 0.4% for NGPCL, 0.6% for abandoned cultivated land, and 1.0% for UA. It was concluded that the classification accuracy of the NGPCL was 84.17, and the kappa was 0.82 (Table 4).

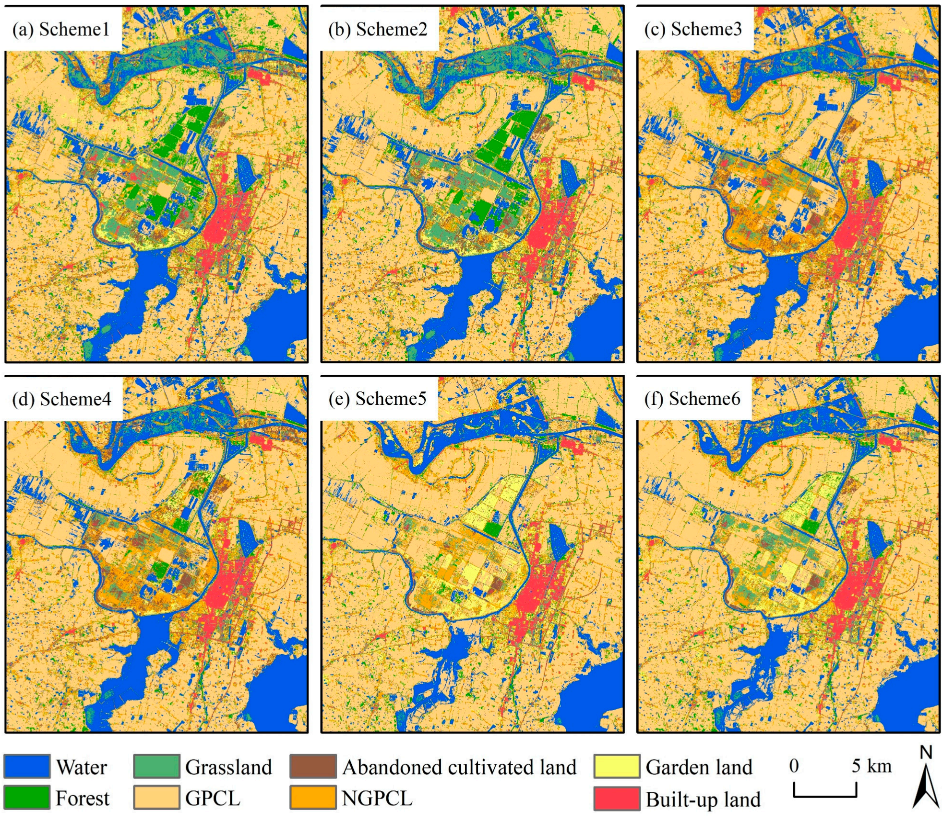

Figure 6. Detailed diagram of classification results of NGPCL using different feature combination schemes.

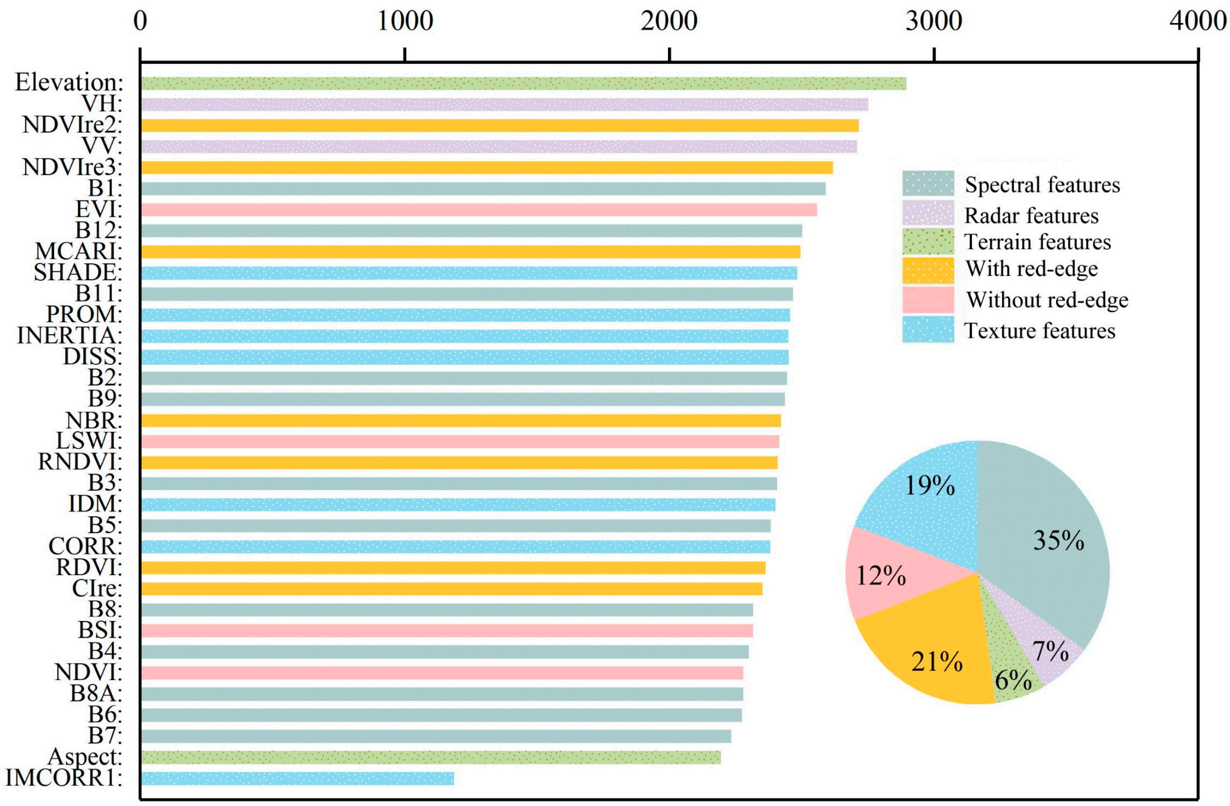

Figure 7. The relative importance of 34 features used for the optimal feature combination scheme (Scheme6).

The results of feature importance (Figure 7) show that spectral features have the highest importance, followed by index features with red edges, texture features, index features without red edges, radar features, and terrain features. This indicates that spectral features play an important role in classification results, and terrain features and radar features also have a high degree of contribution. For the importance of single feature, the top three features are elevation, VH (vertical transmit and horizontal receive), and NDVIre2 (normalized difference vegetation index red-edge2), indicating that elevation was of particular importance for the study area with large terrain variations and the red-edge information of spectral feature was conducive to differentiate land use types.

3.3. Spatial Patterns of NGPCL in Anhui Province

3.3.1. Spatial Distribution Characteristics

The spatial distributions of NGPCL in Anhui province obtained by using the optimal feature combination scheme (Scheme6) are shown in Figure 8 with two typical areas selected for showing details. Generally, the GPCL and NGPCL are effectively identified. The garden land where it is easy to grow grain crops and abandoned cultivated land are also effectively differentiated. As shown in Table 6, the area of land for grain crops is 41,337.6 km^2 while the area of NGPCL is 15,967.2 km^2, accounting for 29.51% and 11.40% of the total area of Anhui province, respectively.

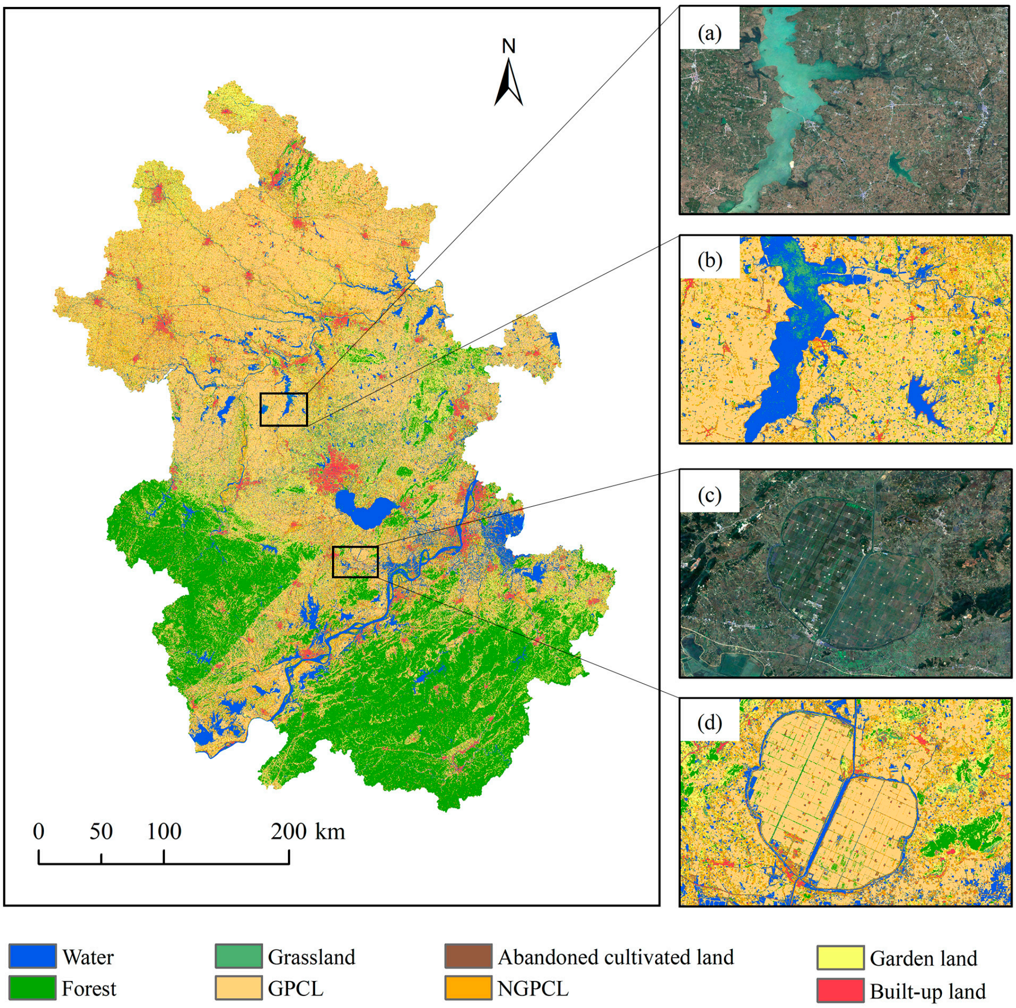

Figure 8. Classification results obtained by using the optimal feature combination scheme (Scheme6); (**b**,**d**) are two typical areas selected for showing details, while (**a**,**c**) are the corresponding remote sensing images of (**b**,**d**), respectively.

Table 6. Classification results using the optimal feature combination scheme (Scheme6) in Anhui province in 2019.

Type	Grassland	Water	Abandoned Cultivated Land	Garden Land	Forest	GPCL	NGPCL	Built-Up Land	Total
Area (km^2)	7170.7	10,515.5	6058.85	20,040.1	33,318	41,337.6	15,967.2	5670.21	140,078.16
Proportion (%)	5.12%	7.51%	4.33%	14.31%	23.79%	29.51%	11.40%	4.05%	100.00%

According to the Ministry of Natural Resources' Special Rectification of the Illegal Occupation of Cultivated Land and actual field surveys, NGPCL could be divided into five types: (1) greening and afforestation on cultivated land; (2) road construction on cultivated land; (3) building ponds on cultivated land; (4) construction of agricultural facilities, such as livestock and aquaculture facilities; and (5) other types that are found by the annual national survey of land resources in China. In this study, 50 pieces of NGPCL were randomly selected from the classification results using the optimal feature combination scheme (Scheme6) to compare with the satellite images on Google Earth pro. Partial results are shown in Figure 9. The classification results using Scheme6 show that NGPCL in Anhui is mostly concentrated on the construction of agricultural facilities (type 4) while a small part is used for construction, such as the construction of rural roads (type 1) and surrounding greening (type 2).

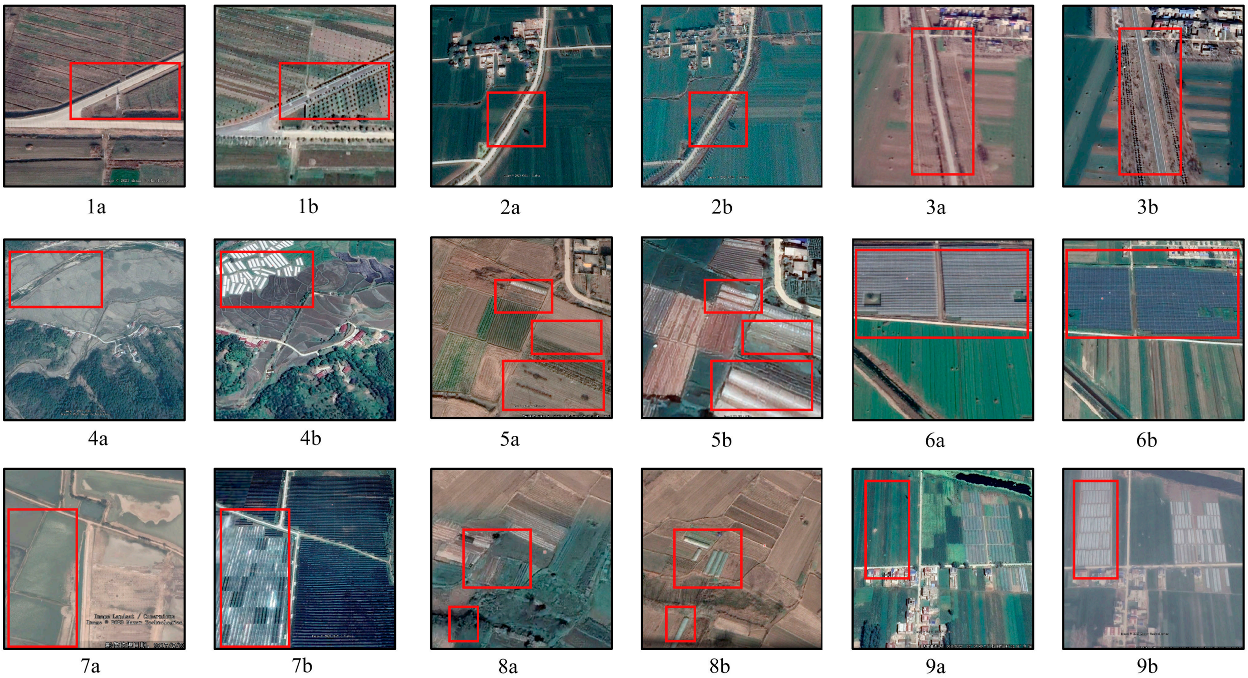

Figure 9. Satellite images taken from Google Earth Pro, showing the different types of transformation from grain production of cultivated land to NGPCL; a and b are a pair of pictures representing the situation of cultivated land before and after the transformation, respectively. Panels 1 and 2 represent greening and afforestation on cultivated land; Panel 3 represents road construction on cultivated land; and Panels 4–9 represent agricultural facility constructions.

The calculated landscape indexes of individual land use types are shown in Figure 10. For the indexes of CA (class area) and LPI (largest patch index), the maximum values are dominated by forest and GPCL, indicating that forest and GPCL were the main land types in the study area. The PD (patch density) values of NGPCL and garden land are relatively higher than those of other landscape types, indicating that NGPCL and garden land are mostly heterogeneous patches with the highest degree of fragmentation.

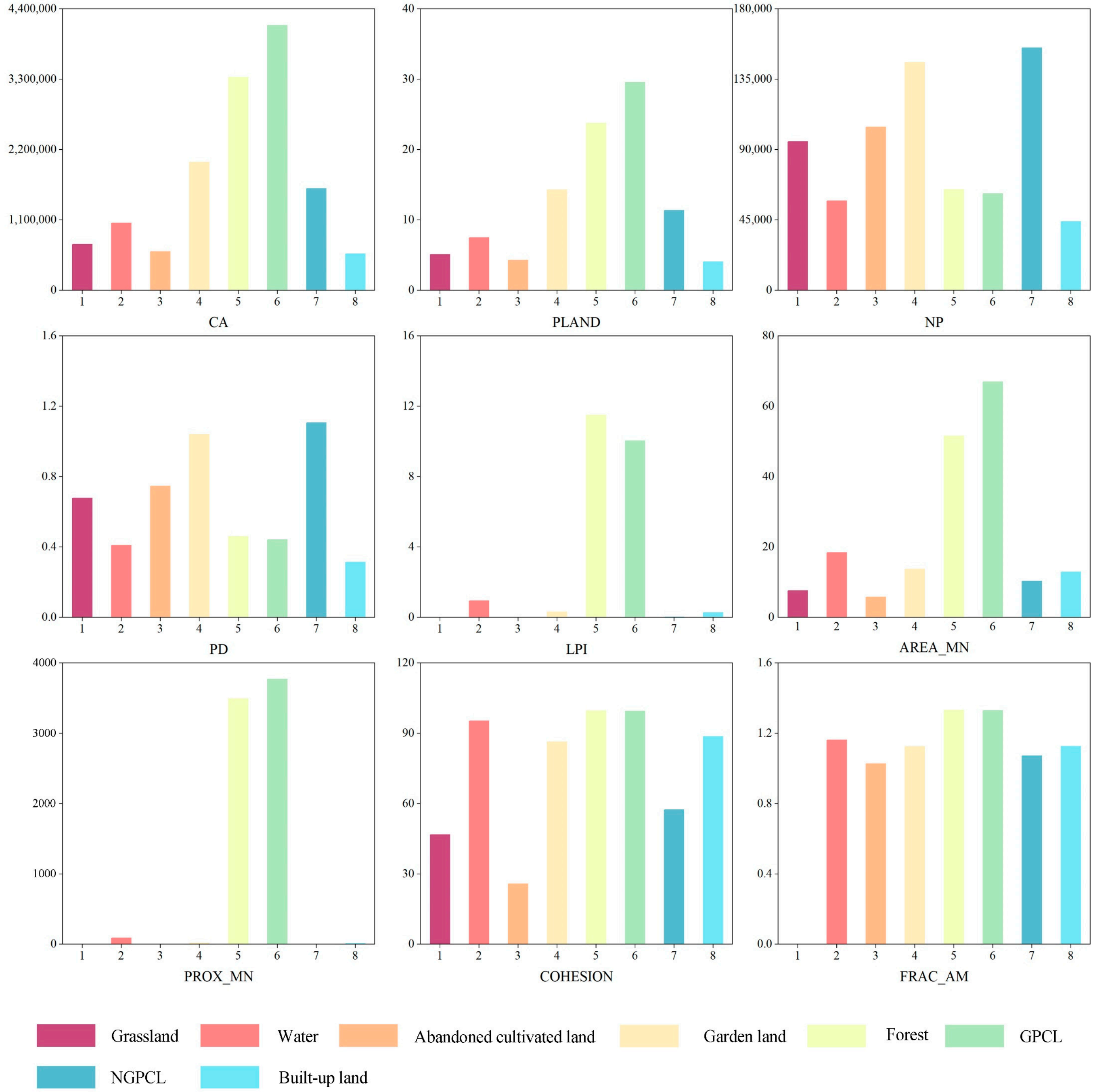

Figure 10. Landscape index at the class level.

3.3.2. Landscape Patterns of NGPCL for Different Terrain Zones

Landscape patterns of NGPCL for different terrain zones in Anhui province are shown in Figure 11 and significant differences are found in the landscape patterns among different terrain zones. Among the four terrain zones, plains and platforms were the dominant terrain types with large areas of NGPCL, indicating that governments should focus on the phenomenon of NGPCL on plains and platforms for solving the problem of NGPCL.

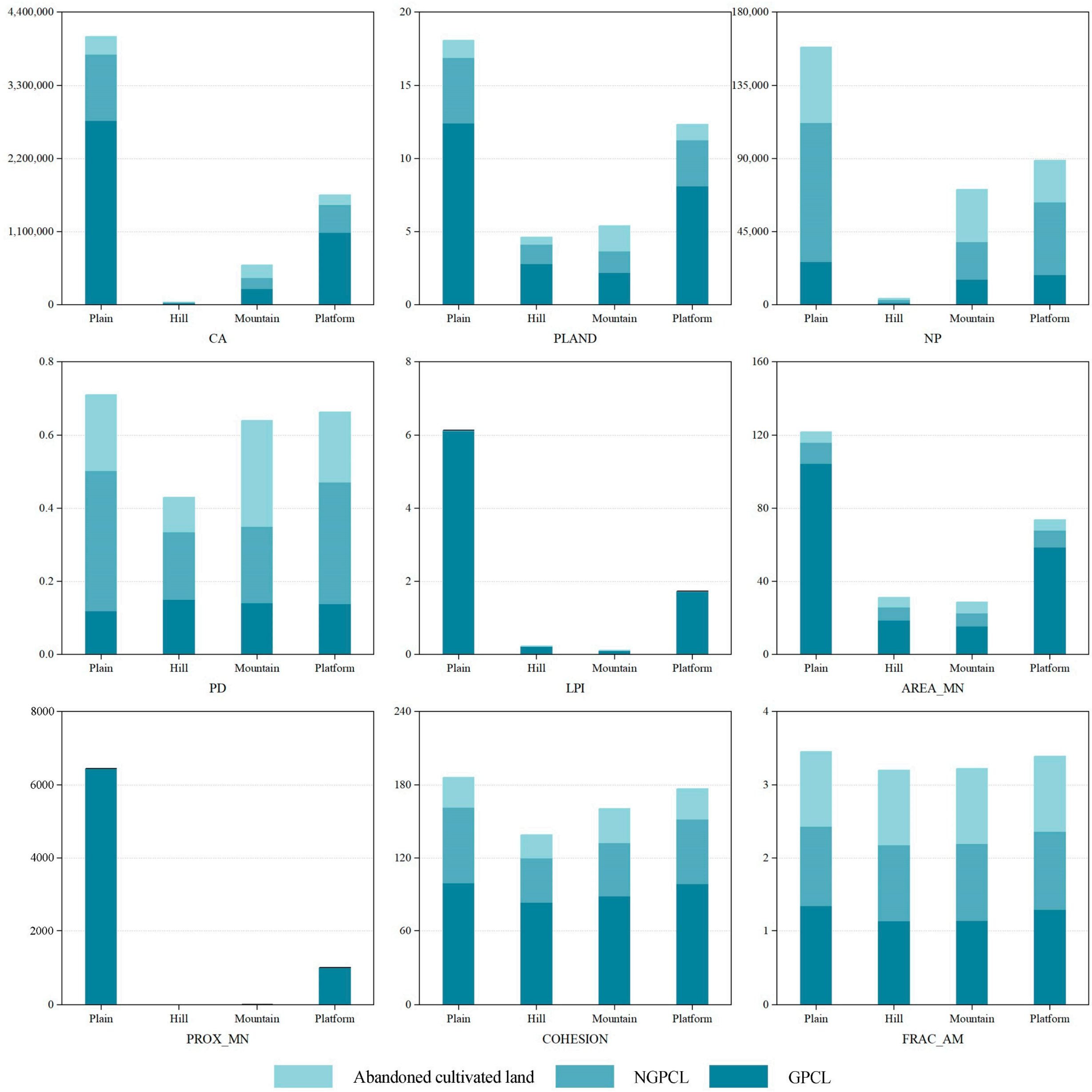

Figure 11. Class-level landscape index for different terrain zones.

The high NP (number of patches) values of NGPCL for three terrain zones of plains, mountain, and platforms demonstrate that the high fragmentation degree and low landscape integrity of NGPCL, indicating that NGPCL may fragment landscape integrity. More attention should be paid to solving the problem of NGPCL for the protection and restoration of landscape ecology and for improving the integrity and connectivity of landscape patterns. In addition, significant differences exist in the maximum patch area (LPI) between different terrain zones. The LPI value of plains is the highest, which indicates that the landscape pattern of GPCL on plains is more continuous and concentrated and serves as the dominant land type. The PROX-MN (proximity index) value for plains and platforms is the highest, indicating high landscape connectivity.

3.3.3. Landscape Patterns of NGPCL for Regions under Different Economic Development Levels

Differences in the landscape patterns of NGPCL for regions under different economic development levels are shown in Figure 12. Significant differences were found in the landscape patterns of NGPCL among regions under different economic development levels, which indicates that significant differences exist in the fragmentation, integrity, and connectivity of different landscape types between different economic development regions. The highest CA value of NGPCL was found in the low economic development region, indicating that the scale of NGPCL in such a region was the largest. However, there was no difference in the proportions of NGPCL to total area of NGPCL, GPCL, and abandoned cultivated land among the three economic development regions, indicating that the problem of NGPCL in Anhui province was prevalent.

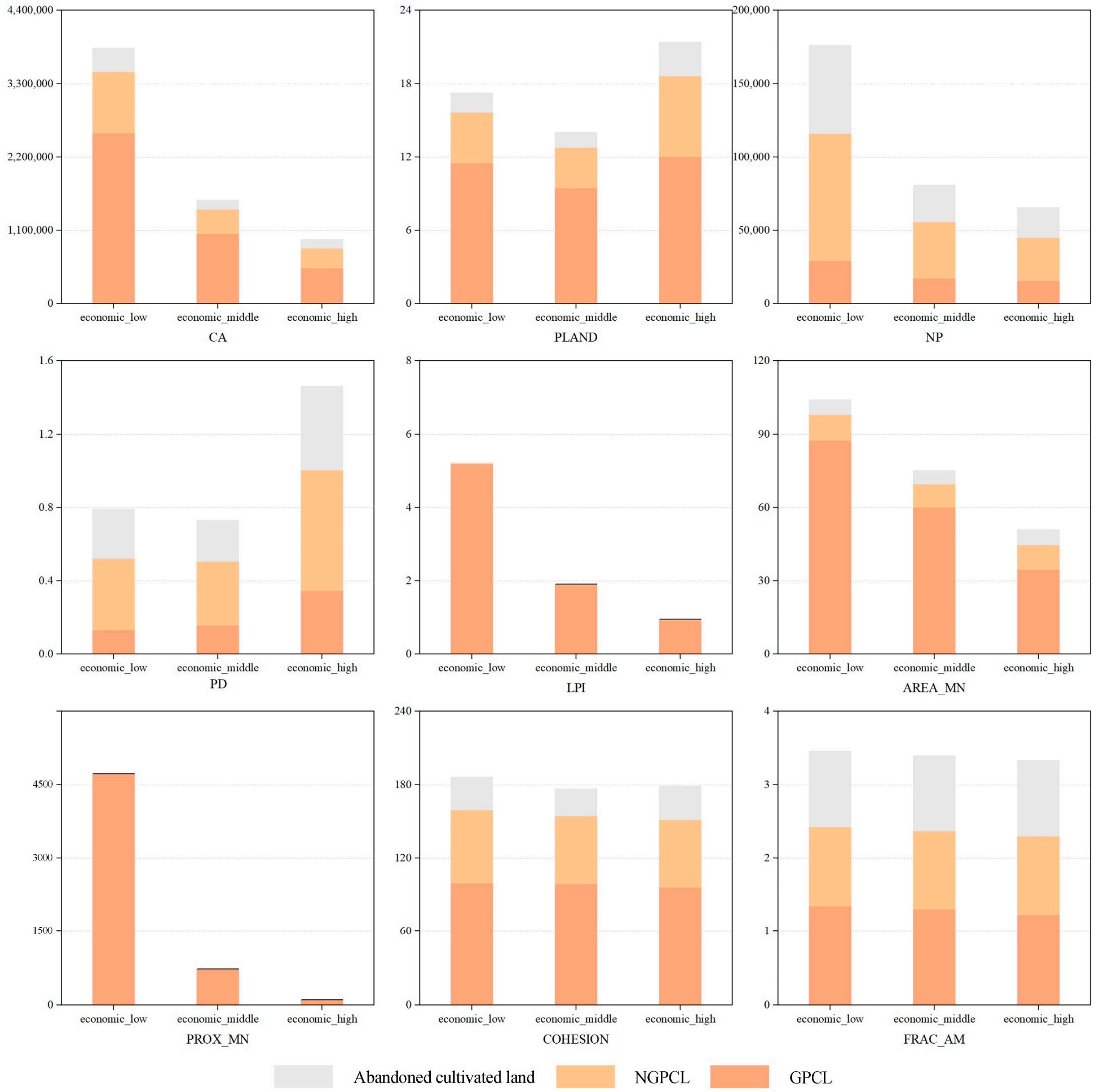

Figure 12. Class-level landscape index for different economic development regions.

Among the three land types of NGPCL, GPCL, and abandoned cultivated land, the highest NP values are found in NGPCL for all three economic development regions, showing that NGPCL in Anhui province has a high degree of fragmentation and a low landscape integrity. Among the three economic development regions, the highest LPI value was found in GPCL in the low economic development region, indicating that the connectivity of GPCL in the low economic development region was better than other economic development regions, which may be related to the low economic development region paying more attention to grain production and the centralized protection of contiguously cultivated land. The highest PROX-MN value of GPCL was also found in the low economic development region, which further proves that the landscape pattern of GPCL in the low economic development region is more connected.

4. Discussion

4.1. Factors Influencing Classification Accuracy

For rapidly and accurately determining NGPCL with low cost on the regional scale, this study integrated a set of technologies to achieve this goal, including the GEE cloud computing platform, the multi-source remote sensing data fusion technique, the machine learning algorithm, and the feature optimization approach, among which, the data fusion technique for integrating SAR (specific absorption rate) data with optical images and the feature optimization approach were of great importance for obtaining the optimal classification model.

Compared with the classification model only using optical images, the classification model combining SAR (specific absorption rate) data with optical images could overcome the limitations of the influence of clouds and rain on classifications using optical images. The SAR data used in this study were not affected by weather conditions because they have a high ability to penetrate clouds, and, thus, directly improve classification accuracy. Compared with single images, multi-temporal images can obtain abundant phenological characteristics of crops, which effectively reduce crop misclassification and omission, and improve crop classification accuracy. Combining multitemporal SAR data with multitemporal optical images was adopted in this study and was an effective method of obtaining accurate and comprehensive crop information. This method has broad application prospects in the fields of agriculture, land use, and environmental monitoring, and provides a valuable reference for crop growth monitoring, yield estimation, and agricultural resources management.

However, a larger number of features used in a classification model is not always better because redundancy and invalid and conflicting information may exist in these features [55,56]. Feature optimization is an effective means to reduce feature redundancy and conflict information [14]. Common feature optimization methods include J-M distance, principal component analysis, and other methods. This study uses the operator-explain function provided by the GEE cloud platform to measure the importance of individual features. In this study, a total of 57 features were collected in the classification comparison. By using the feature optimization approach, the number of features used in classification was significantly reduced from 57 to 34, a decrease of 40.4%, which not only improved classification accuracy and classification efficiency, but also reduced the redundancy of feature information and enhanced the scientific interpretability.

4.2. Potential Policy Implications for Land Resources Management

Faced with the problem of NGPCL that is gradually expanding, it is often difficult to implement a simple "one size fits all" prohibition strategy in actual management [57]. The management policies proposed to constrain the trend of NGPCL mainly include improving the compensation policies for cultivated land protection at the national level (such as increasing the compensation for cultivated land protection and establishing a cross-regional protection and compensation mechanism for cultivated land), strengthening the government's responsibility for supervising GPCL, modifying policies to benefit farmers (such as increasing grain prices and improving grain-growing subsidy policies), regulating rural land transfer, and developing arable land supervision systems to strengthen the supervision of arable land use [58–61]. However, the management and regulation strategies of NGPCL should be in accordance with the differences in development goals. However, previous studies usually neglect the different types of NGPCL. Therefore, further research is urgently needed to propose standardized and differentiated policies for preventing the trend of NGPCL [14,62].

Under the background of the national policy of strictly preventing the occurrence of NGPCL, Anhui province has formulated relevant detailed measures. In March 2021, the Anhui Provincial People's Government issued a policy interpretation of the "Anhui Provincial Work Plan for Preventing Non-grain Transformation of Farmland and Stabilizing Grain Production", which emphasized the priority of the use of cultivated land resources, and emphasized that permanent basic cultivated land should be used to develop grain crops. Generally, cultivated land should be mainly used for the production of edible agricultural products, such as grain, oilseeds, vegetables, forage, and fodder; regarding the security of the supply of food and edible agricultural products, cultivated land is allowed to be moderately used for the production of non-edible agricultural products. Since appropriate use of agricultural facilities on cultivated land is conducive to local economic development, NGPCL that mostly occurs in Anhui province, such as the construction of agricultural facilities, still exists despite years of publicity and the implementation of legal procedures such as "submitting for approval and filing".

Accurately and rapidly monitoring NGPCL is an important prerequisite for precise control of NGPCL; the remote sensing monitoring approach used in this study can detect illegal patches of NGPCL in time. Taking Anhui province as a unit, the free Sentinel-2 satellite remote sensing images (10 m resolution) on the GEE cloud platform are used to achieve the dynamic monitoring of NGPCL every five days, which could help to realize the early identification and early intervention of NGPCL. Moreover, such a remote sensing monitoring approach could provide technical support for relevant departments to conduct land law enforcement.

Moreover, the results of this study show that the phenomenon of NGPCL is more likely to occur in plains and the economically developed areas; however, the current poli-cy does not address the balance between farmers' income and the effective protection of cultivated land across different regions. Therefore, governments should formulate differentiated policies for preventing the occurrence of NGPCL. Furthermore, measures such as scientific planning of land use arrangements, including NGPCL, are conducive to preventing the disorderly occurrence of NGPCL.

5. Conclusions

This study determined the spatial distributions of NGPCL by means of remote sensing monitoring and analyzed the spatial patterns of NGPCL in Anhui province in 2019. Specifically, this study focused on the development of classification approach which combines the use of multi-source remote sensing data, random forest algorithm, feature optimization approach, and GEE cloud platform, which proved to be an effective tool that could rapidly and accurately identify the spatial distributions of NGPCL patches on a regional scale. The results show that terrain features, radar features, and texture features help the identification of NGPCL. Additionally, the feature optimization approach could improve classification accuracy and efficiency, and scientific interpretability by eliminating redundancy and conflicts between different features. The results also indicate that the phenomenon of NGPCL in Anhui province is more likely to occur in the economically developed areas and in plains, and cultivated land used for planting grain crops and used for non-grain crops at the county level usually presents clustered spatial autocorrelation relationships. Such a finding underscores the urgent need to formulate differentiated policies for preventing the phenomenon of NGPCL. This research is of great importance to rapidly remote sensing monitoring of the occurrence of NGPCL on a regional or national scale and to the efficient management of cultivated land resources. Although a high-performance classification model has been built to determine NGPCL on a large scale, the classification model needs to be further modified for improving the classification accuracy. Future work intends to use the differentiated phenological information between different vegetation and to replace the random forest algorithm with a deep learning algorithm which has been demonstrated with higher performance in various fields. Additionally, future work should pay more attention to the formulation of differentiated policies for preventing the occurrence of NGPCL.

Author Contributions: Conceptualization, J.Z. and W.L.; methodology, J.Z.; software, X.C., Y.S., D.X., C.D., L.J., J.W., Z.Z., S.L., Y.L. and G.Z.; validation, J.Z. and X.C.; formal analysis, J.Z. and Y.S.; investigation, X.C., D.X. and C.D.; resources, W.L.; data curation, W.L.; writing—original draft, J.Z.; writing—review and editing, J.Z.; visualization, X.C., Y.S., D.X., C.D., L.J. and J.W.; supervision, Z.Z., S.L., Y.L. and G.Z.; project administration, J.Z. and W.L.; funding acquisition, J.Z. and W.L. All authors have read and agreed to the published version of the manuscript.

Funding: This research was funded by the MOE (Ministry of Education in China) Youth Foundation Project of Humanities and Social Sciences (grant no. 21YJCZH243), the Natural Science Foundation of China (no. 42271060), the Natural Science Foundation of Anhui province (no. 2208085MD91), the Open Fund of the Key Laboratory of Jianghuai Arable Land Resources Protection and Eco-restoration, the Ministry of Natural Resources (no. 2022-ARPE-KF01), the Anhui University Scientific Research Project (no. YJS20210184), and the Undergraduate Innovation and Entrepreneurship Training Program of Anhui Normal University (no. 202210370002).

Data Availability Statement: Not applicable.

Conflicts of Interest: The authors declare no conflict of interest.

References

1. Ran, D.; Zhang, Z.; Jing, Y. A Study on the Spatial–Temporal Evolution and Driving Factors of Non-Grain Production in China's Major Grain-Producing Provinces. *Int. J. Environ. Res. Public Health* **2022**, *19*, 16630. [CrossRef]
2. Zhou, Y.; Li, X.; Liu, Y. Cultivated Land Protection and Rational Use in China. *Land Use Policy* **2021**, *106*, 105454. [CrossRef]
3. FAO; IFAD; UNICEF; WFP; WHO. *The State of Food Security and Nutrition in the World 2021*; FAO: Rome, Italy, 2021; ISBN 978-92-5-134325-8.
4. Sadigov, R. Rapid Growth of the World Population and Its Socioeconomic Results. *Sci. World J.* **2022**, *2022*, 8110229. [CrossRef]
5. Zhang, D.; Yang, W.; Kang, D.; Zhang, H. Spatial-Temporal Characteristics and Policy Implication for Non-Grain Production of Cultivated Land in Guanzhong Region. *Land Use Policy* **2023**, *125*, 106466. [CrossRef]
6. Su, Y.; He, S.; Wang, K.; Shahtahmassebi, A.R.; Zhang, L.; Zhang, J.; Zhang, M.; Gan, M. Quantifying the Sustainability of Three Types of Agricultural Production in China: An Emergy Analysis with the Integration of Environmental Pollution. *J. Clean. Prod.* **2020**, *252*, 119650. [CrossRef]
7. Cheng, X.; Tao, Y.; Huang, C.; Yi, J.; Yi, D.; Wang, F.; Tao, Q.; Xi, H.; Ou, W. Unraveling the Causal Mechanisms for Non-Grain Production of Cultivated Land: An Analysis Framework Applied in Liyang, China. *Land* **2022**, *11*, 1888. [CrossRef]
8. Guo, Y.; Wang, J. Identifying the Determinants of Nongrain Farming in China and Its Implications for Agricultural Development. *Land* **2021**, *10*, 902. [CrossRef]
9. Lark, T.J.; Schelly, I.H.; Gibbs, H.K. Accuracy, Bias, and Improvements in Mapping Crops and Cropland across the United States Using the USDA Cropland Data Layer. *Remote Sens.* **2021**, *13*, 968. [CrossRef]
10. Hu, Q.; Wu, W.; Song, Q.; Yu, Q.; Yang, P.; Tang, H. Recent Progresses in Research of Crop Patterns Mapping by Using Remote Sensing. *Sci. Agric. Sin.* **2015**, *48*, 1900–1914. [CrossRef]
11. Liang, X.; Jin, X.; Liu, J.; Yin, Y.; Gu, Z.; Zhang, J.; Zhou, Y. Formation Mechanism and Sustainable Productivity Impacts of Non-grain Croplands: Evidence from Sichuan Province, China. *Land Degrad. Dev.* **2023**, *34*, 1120–1132. [CrossRef]
12. Li, J.; Zhou, K.; Dong, H.; Xie, B. Cultivated Land Change, Driving Forces and Its Impact on Landscape Pattern Changes in the Dongting Lake Basin. *Int. J. Environ. Res. Public Health* **2020**, *17*, 7988. [CrossRef]
13. Portalés-Julià, E.; Campos-Taberner, M.; García-Haro, F.J.; Gilabert, M.A. Assessing the Sentinel-2 Capabilities to Identify Abandoned Crops Using Deep Learning. *Agronomy* **2021**, *11*, 654. [CrossRef]
14. Su, Y.; Qian, K.; Lin, L.; Wang, K.; Guan, T.; Gan, M. Identifying the Driving Forces of Non-Grain Production Expansion in Rural China and Its Implications for Policies on Cultivated Land Protection. *Land Use Policy* **2020**, *92*, 104435. [CrossRef]
15. Liu, G.; Zhao, L.; Chen, H.; Zhou, Y.; Lin, H.; Wang, C.; Huang, H.; Li, X.; Yuan, Z. Does Farmland Transfer Lead to Non-Grain Production in Agriculture?—An Empirical Analysis Based on the Differentiation of Farmland Renting-In Objects. *Sustainability* **2022**, *15*, 379. [CrossRef]
16. Yin, H.; Brandão, A.; Buchner, J.; Helmers, D.; Iuliano, B.G.; Kimambo, N.E.; Lewińska, K.E.; Razenkova, E.; Rizayeva, A.; Rogova, N.; et al. Monitoring Cropland Abandonment with Landsat Time Series. *Remote Sens. Environ.* **2020**, *246*, 111873. [CrossRef]
17. Qiu, T.; Boris Choy, S.T.; Li, S.; He, Q.; Luo, B. Does Land Renting-in Reduce Grain Production? Evidence from Rural China. *Land Use Policy* **2020**, *90*, 104311. [CrossRef]
18. Yi, F.; Sun, D.; Zhou, Y. Grain Subsidy, Liquidity Constraints and Food Security—Impact of the Grain Subsidy Program on the Grain-Sown Areas in China. *Food Policy* **2015**, *50*, 114–124. [CrossRef]
19. Li, Y.; Zhao, B.; Huang, A.; Xiong, B.; Song, C. Characteristics and Driving Forces of Non-Grain Production of Cultivated Land from the Perspective of Food Security. *Sustainability* **2021**, *13*, 14047. [CrossRef]
20. Liu, Y.; Zhou, Y. Reflections on China's Food Security and Land Use Policy under Rapid Urbanization. *Land Use Policy* **2021**, *109*, 105699. [CrossRef]

21. Liu, X.; Zhao, C.; Song, W. Review of the Evolution of Cultivated Land Protection Policies in the Period Following China's Reform and Liberalization. *Land Use Policy* **2017**, *67*, 660–669. [CrossRef]
22. Yang, H. Land Conservation Campaign in China: Integrated Management, Local Participation and Food Supply Option. *Geoforum* **2004**, *35*, 507–518. [CrossRef]
23. Li, W.; Feng, T.; Hao, J. The Evolving Concepts of Land Administration in China: Cultivated Land Protection Perspective. *Land Use Policy* **2009**, *26*, 262–272. [CrossRef]
24. Deng, X.; Huang, J.; Rozelle, S.; Zhang, J.; Li, Z. Impact of Urbanization on Cultivated Land Changes in China. *Land Use Policy* **2015**, *45*, 1–7. [CrossRef]
25. You, N.; Dong, J. Examining Earliest Identifiable Timing of Crops Using All Available Sentinel 1/2 Imagery and Google Earth Engine. *ISPRS J. Photogramm. Remote Sens.* **2020**, *161*, 109–123. [CrossRef]
26. Su, Y.; Li, C.; Wang, K.; Deng, J.; Shahtahmassebi, A.R.; Zhang, L.; Ao, W.; Guan, T.; Pan, Y.; Gan, M. Quantifying the Spatiotemporal Dynamics and Multi-Aspect Performance of Non-Grain Production during 2000–2015 at a Fine Scale. *Ecol. Indic.* **2019**, *101*, 410–419. [CrossRef]
27. Wang, J.; Zhang, Z.; Liu, Y. Spatial Shifts in Grain Production Increases in China and Implications for Food Security. *Land Use Policy* **2018**, *74*, 204–213. [CrossRef]
28. He, Y.; Dong, J.; Liao, X.; Sun, L.; Wang, Z.; You, N.; Li, Z.; Fu, P. Examining Rice Distribution and Cropping Intensity in a Mixed Single- and Double-Cropping Region in South China Using All Available Sentinel 1/2 Images. *Int. J. Appl. Earth Obs. Geoinf.* **2021**, *101*, 102351. [CrossRef]
29. Shahtahmassebi, A.R.; Li, C.; Fan, Y.; Wu, Y.; Lin, Y.; Gan, M.; Wang, K.; Malik, A.; Blackburn, G.A. Remote Sensing of Urban Green Spaces: A Review. *Urban For. Urban Green.* **2021**, *57*, 126946. [CrossRef]
30. Shojanoori, R.; Shafri, H.Z.M.; Mansor, S.; Ismail, M.H. Generic Rule-Sets for Automated Detection of Urban Tree Species from Very High-Resolution Satellite Data. *Geocarto Int.* **2018**, *33*, 357–374. [CrossRef]
31. Phalke, A.R.; Özdoğan, M.; Thenkabail, P.S.; Erickson, T.; Gorelick, N.; Yadav, K.; Congalton, R.G. Mapping Croplands of Europe, Middle East, Russia, and Central Asia Using Landsat, Random Forest, and Google Earth Engine. *ISPRS J. Photogramm. Remote Sens.* **2020**, *167*, 104–122. [CrossRef]
32. Motohka, T.; Nasahara, K.N.; Murakami, K.; Nagai, S. Evaluation of Sub-Pixel Cloud Noises on MODIS Daily Spectral Indices Based on in Situ Measurements. *Remote Sens.* **2011**, *3*, 1644–1662. [CrossRef]
33. Du, Y.; Zhang, Y.; Ling, F.; Wang, Q.; Li, W.; Li, X. Water Bodies' Mapping from Sentinel-2 Imagery with Modified Normalized Difference Water Index at 10-m Spatial Resolution Produced by Sharpening the SWIR Band. *Remote Sens.* **2016**, *8*, 354. [CrossRef]
34. Zhang, Y.; Odeh, I.O.A.; Han, C. Bi-Temporal Characterization of Land Surface Temperature in Relation to Impervious Surface Area, NDVI and NDBI, Using a Sub-Pixel Image Analysis. *Int. J. Appl. Earth Obs. Geoinf.* **2009**, *11*, 256–264. [CrossRef]
35. Faridatul, M.I.; Wu, B. Automatic Classification of Major Urban Land Covers Based on Novel Spectral Indices. *ISPRS Int. J. Geo-Inf.* **2018**, *7*, 453. [CrossRef]
36. Wei, P.; Zhu, W.; Zhao, Y.; Fang, P.; Zhang, X.; Yan, N.; Zhao, H. Extraction of Kenyan Grassland Information Using PROBA-V Based on RFE-RF Algorithm. *Remote Sens.* **2021**, *13*, 4762. [CrossRef]
37. Xu, L.Y.; Xie, X.D.; Li, S. Correlation Analysis of the Urban Heat Island Effect and the Spatial and Temporal Distribution of Atmospheric Particulates Using TM Images in Beijing. *Environ. Pollut.* **2013**, *178*, 102–114. [CrossRef]
38. Wang, Z.; Yao, F.; Li, W.; Wu, A.J. Saturation Correction for Nighttime Lights Data Based on the Relative NDVI. *Remote Sens.* **2017**, *9*, 759. [CrossRef]
39. Zhang, J.; Liu, X.; Liang, Y.; Cao, Q.; Tian, Y.; Zhu, Y.; Cao, W.; Liu, X. Using a Portable Active Sensor to Monitor Growth Parameters and Predict Grain Yield of Winter Wheat. *Sensors* **2019**, *19*, 1108. [CrossRef]
40. Shen, Y.; Li, Q.Z.; Du, X.; Wang, H.Y.; Zhang, Y. Indicative Features for Identifying Corn and Soybean Using Remote Sensing Imagery at Middle and Later Growth Season. *Natl. Remote Sens. Bull.* **2022**, *26*, 1410–1422. [CrossRef]
41. Ning, X.G.; Chang, W.T.; Wang, H.; Zhang, H.C.; Zhu, Q.D. Extraction of Marsh Wetland in Heilongjiang Basin Based on GEE and Multi-Source Remote Sensing Data. *Natl. Remote Sens. Bull.* **2022**, *26*, 386–396. [CrossRef]
42. Tiwari, A.; Suozzi, E.; Silva, C.; De Maio, M.; Zanetti, M. Role of Integrated Approaches in Water Resources Management: Antofagasta Region, Chile. *Sustainability* **2021**, *13*, 1297. [CrossRef]
43. Fan, S.; Zhang, B.; Mouche, A.A.; Perrie, W.; Zhang, J.A.; Zhang, G. Estimation of Wind Direction in Tropical Cyclones Using C-Band Dual-Polarization Synthetic Aperture Radar. *IEEE Trans. Geosci. Remote Sens.* **2020**, *58*, 1450–1462. [CrossRef]
44. Al-Janobi, A. Performance Evaluation of Cross-Diagonal Texture Matrix Method of Texture Analysis. *Pattern Recognit.* **2001**, *34*, 171–180. [CrossRef]
45. Khojastehnazhand, M.; Roostaei, M. Classification of Seven Iranian Wheat Varieties Using Texture Features. *Expert Syst. Appl.* **2022**, *199*, 117014. [CrossRef]
46. Sun, J.; Zhong, G.; Huang, K.; Dong, J. Banzhaf Random Forests: Cooperative Game Theory Based Random Forests with Consistency. *Neural Netw.* **2018**, *106*, 20–29. [CrossRef] [PubMed]
47. Sudiana, D.; Lestari, A.I.; Riyanto, I.; Rizkinia, M.; Arief, R.; Prabuwono, A.S.; Sri Sumantyo, J.T. A Hybrid Convolutional Neural Network and Random Forest for Burned Area Identification with Optical and Synthetic Aperture Radar (SAR) Data. *Remote Sens.* **2023**, *15*, 728. [CrossRef]

48. Pan, T.; Zuo, R.; Wang, Z. Geological Mapping via Convolutional Neural Network Based on Remote Sensing and Geochemical Survey Data in Vegetation Coverage Areas. *IEEE J. Sel. Top. Appl. Earth Obs. Remote Sens.* **2023**, *16*, 3485–3494. [CrossRef]
49. Belgiu, M.; Drăguţ, L. Random Forest in Remote Sensing: A Review of Applications and Future Directions. *ISPRS J. Photogramm. Remote Sens.* **2016**, *114*, 24–31. [CrossRef]
50. Maimaitiyiming, M.; Ghulam, A.; Tiyip, T.; Pla, F.; Latorre-Carmona, P.; Halik, Ü.; Sawut, M.; Caetano, M. Effects of Green Space Spatial Pattern on Land Surface Temperature: Implications for Sustainable Urban Planning and Climate Change Adaptation. *ISPRS J. Photogramm. Remote Sens.* **2014**, *89*, 59–66. [CrossRef]
51. Inkoom, J.N.; Frank, S.; Greve, K.; Walz, U.; Fürst, C. Suitability of Different Landscape Metrics for the Assessments of Patchy Landscapes in West Africa. *Ecol. Indic.* **2018**, *85*, 117–127. [CrossRef]
52. Chen, W.B.; Xiao, D.N.; Li, X.Z. Classification, Application, and Creation of Landscape Indices. *Chin. J. Appl. Ecol.* **2002**, *13*, 121–125.
53. Yeh, C.-T.; Huang, S.-L. Investigating Spatiotemporal Patterns of Landscape Diversity in Response to Urbanization. *Landsc. Urban Plan.* **2009**, *93*, 151–162. [CrossRef]
54. Huang, D.; Xu, S.; Sun, J.; Liang, S.; Song, W.; Wang, Z. Accuracy Assessment Model for Classification Result of Remote Sensing Image Based on Spatial Sampling. *J. Appl. Remote Sens* **2017**, *11*, 046023. [CrossRef]
55. Bai, Y.; Sun, G.; Li, Y.; Ma, P.; Li, G.; Zhang, Y. Comprehensively Analyzing Optical and Polarimetric SAR Features for Land-Use/Land-Cover Classification and Urban Vegetation Extraction in Highly-Dense Urban Area. *Int. J. Appl. Earth Obs. Geoinf.* **2021**, *103*, 102496. [CrossRef]
56. Dobrinić, D.; Gašparović, M.; Medak, D. Sentinel-1 and 2 Time-Series for Vegetation Mapping Using Random Forest Classification: A Case Study of Northern Croatia. *Remote Sens.* **2021**, *13*, 2321. [CrossRef]
57. Kong, X. The Problem, Causes and Countermeasures of "Non Grain Conversion" of Cultivated Land. *China Land* **2020**, *418*, 17–19. [CrossRef]
58. Wu, S.C.; Yu, H.L.; Chu, Y.F. Limitations and Breakthroughs in the Study of "Non Grain" in Cultivated Land Under Agricultural Scale Management. *J. Northwest A&F Univ. (Soc. Sci. Ed.)* **2019**, *19*, 142–151. [CrossRef]
59. Liang, X.Y.; Jin, X.B.; Sun, R.; Han, B.; Ren, J.; Zhou, Y.K. China's Resilience-Space for Cultivated Land Protection under the Restraint of Multi-Scenario Food Security Bottom Line. *Acta Geogr. Sin.* **2022**, *77*, 697–713.
60. Han, X.; Xue, P.; Zhang, N. Impact of Grain Subsidy Reform on the Land Use of Smallholder Farms: Evidence from Huang-Huai-Hai Plain in China. *Land* **2021**, *10*, 929. [CrossRef]
61. Su, M.; Guo, R.; Hong, W. Institutional Transition and Implementation Path for Cultivated Land Protection in Highly Urbanized Regions: A Case Study of Shenzhen, China. *Land Use Policy* **2019**, *81*, 493–501. [CrossRef]
62. Zhang, Y.W.; Lu, X.H. The Impact of Differentiated Policy Tools on the Cultivated Land Protection Effects. *Resour. Sci.* **2022**, *44*, 660–673.